Spontaneous Self-Assembly of Perovskite Nanocrystals into Electronically Coupled Supercrystals: Toward Filling the Green Gap

Yu Tong, En-Ping Yao, Aurora Manzi, Eva Bladt, Kun Wang, Markus Döblinger, Sara Bals, Peter Müller-Buschbaum, Alexander S. Urban, Lakshminarayana Polavarapu, and Jochen Feldmann*

Self-assembly of nanoscale building blocks into ordered nanoarchitectures has emerged as a simple and powerful approach for tailoring the nanoscale properties and the opportunities of using these properties for the development of novel optoelectronic nanodevices. Here, the one-pot synthesis of $CsPbBr_3$ perovskite supercrystals (SCs) in a colloidal dispersion by ultrasonication is reported. The growth of the SCs occurs through the spontaneous self-assembly of individual nanocrystals (NCs), which form in highly concentrated solutions of precursor powders. The SCs retain the high photoluminescence (PL) efficiency of their NC subunits, however also exhibit a redshifted emission wavelength compared to that of the individual nanocubes due to interparticle electronic coupling. This redshift makes the SCs pure green emitters with PL maxima at ≈530–535 nm, while the individual nanocubes emit a cyan-green color (≈512 nm). The SCs can be used as an emissive layer in the fabrication of pure green light-emitting devices on rigid or flexible substrates. Moreover, the PL emission color is tunable across the visible range by employing a well-established halide ion exchange reaction on the obtained $CsPbBr_3$ SCs. These results highlight the promise of perovskite SCs for light emitting applications, while providing insight into their collective optical properties.

Recently, metal halide perovskites have created a great deal of excitement especially for solar energy conversion applications based on their outstanding optical and optoelectronic properties.[1–7] Consequently, this promising material has been explored for many uses, such as light-emitting diodes (LEDs), lasers, photodetectors, and photovoltaics.[8–10] For light emission, it has been shown that lower dimensional nanocrystals (NCs) provide far superior performances and tunability than their bulk counterparts.[11–18] In particular, colloidal cesium lead halide ($CsPbX_3$, X = Cl, Br, and I) perovskite NCs have shifted to the center of attention as they exhibit higher stability as well as extremely high photoluminescence quantum yields (PLQYs) (≈80–100%) compared to organic-inorganic hybrid perovskites.[8,19–21] The optical properties of perovskite NCs are generally tunable across the entire visible range by controlling the halide composition[22–24] and dimensionality.[24–26] Many groups have also been investigating a wide range of morphologies such as nanocubes, nanoplatelets, and nanowires in order to determine their effect on the optical properties of the NCs.[26–31] Despite the rapid advances of low dimensional $CsPbBr_3$ perovskite NCs, achieving a pure green emission with high quantum efficiency is still challenging. Generally, the NCs are employed as phosphors, absorbing blue light emitted from a solid state LED and emitting in the yellow or green and red to replicate white light.[32,33] Also, while they typically far outperform the bulk thin films in terms of light emission, they are only weakly emitting in the blue and currently cannot replicate a true green emission, which would be essential for closing the so-called "green gap."[24,34,35]

Y. Tong, Dr. E.-P. Yao, A. Manzi, Dr. A. S. Urban, Dr. L. Polavarapu, Prof. J. Feldmann
Chair for Photonics and Optoelectronics
Department of Physics and Center for NanoScience (CeNS)
Ludwig-Maximilians-Universität München
Amalienstr. 54, 80799 Munich, Germany
E-mail: l.polavarapu@lmu.de

Y. Tong, Dr. E.-P. Yao, A. Manzi, K. Wang, Prof. P. Müller-Buschbaum, Dr. A. S. Urban, Dr. L. Polavarapu, Prof. J. Feldmann
Nanosystems Initiative Munich (NIM)
Schellingstr. 4, 80799 Munich, Germany

Dr. E. Bladt, Prof. S. Bals
EMAT
University of Antwerp
Groenenborgerlaan 171, B-2020 Antwerp, Belgium

K. Wang, Prof. P. Müller-Buschbaum
Technische Universität München
Physik-Department
Lehrstuhl für Funktionelle Materialien
James-Franck-Str. 1, 85748 Garching, Germany

Dr. M. Döblinger
Department of Chemistry
Ludwig-Maximilians-Universität München
Butenandtstr. 11, 81377 Munich, Germany

DOI: 10.1002/adma.201801117

One of the reasons for the reduced PLQY in bulk structures lies in the nature of the long diffusion length of charge carriers in perovskites. Once created they have a large chance of diffusing to a trap state in the crystal and undergoing subsequent nonradiative recombination.[31] One possibility to work around this problem could be to start with high PLQY NCs and couple them together electronically. The electronic coupling, while leading to a redshift of the PL, could limit the diffusion length of the carriers, thereby significantly reducing the probability for trap-assisted recombination. This can be achieved through the self-assembly of NCs into supercrystals (SCs)/superlattices, exhibiting a miniband formation in both valence and conduction bands.[36–39] Such miniband formation has been observed previously in conventional semiconductors such as GaAs superlattices[36] and aggregated CdTe NCs,[39] however it has yet to be realized in perovskites. The self-assembly process itself, which has been extensively used to control the properties of metal, magnetic and conventional semiconductor NCs, presents an interesting way of bringing the NCs together in such a desired manner.[40–45] This process is typically accomplished by several methods: 1) slow solvent evaporation of the concentrated colloidal NC solution on a solid substrate, 2) via self-assembly at air/liquid or liquid/liquid interfaces, and 3) through intermolecular interactions between ligands of the NC surface. Importantly, the morphology and monodispersity of NCs play a crucial role in the formation of ordered assemblies. Despite significant advances in the self-assembly of metal and conventional semiconductor NCs into one-dimensional (1D), 2D, and 3D superlattices,[40–44] very few attempts have been made to date toward the realization of perovskite self-assemblies and understanding their ensemble properties.[2,31,46]

Herein, we report on the spontaneous self-assembly of $CsPbBr_3$ perovskite NCs into highly luminescent colloidal 3D SCs in a one-pot colloidal synthesis from a concentrated precursor solution. It was found that the SCs exhibit a redshifted emission compared to the fluorescence of individual $CsPbBr_3$ NCs due to interparticle electronic coupling, yet retain the high PL quantum yields of the individual NCs. The redshift makes the SCs pure green emitters (530–535 nm), while the individual $CsPbBr_3$ NCs exhibit only blue-green emission (510–515 nm). This is particularly promising for television display applications as per Rec2020 color standards. The emission color of SCs can be tuned across the visible light spectrum by varying the halide ion (Br^-, Cl^-, and I^-) composition through typical halide ion exchange reaction.[22,23] We demonstrate the applicability of the SCs by fabricating pure green electroluminescent devices (≈530 nm).

The synthesis was based on the findings from our previous study, in which perovskite NCs were synthesized directly from precursor salts by ultrasonication.[24] In this work, we added the precursor salts (Cs_2CO_3 and $PbBr_2$) to octadecene in the presence of oleic acid and oleylamine, however increased their concentration by ten times (**Figure 1**a; Figure S1, Supporting Information). While the solution color turned into bright yellow, as in the case of the formed NCs, the solution became opaque and quickly, perovskite material precipitation was observed on the bottom of the vials, indicating the presence of large particles. To investigate this, we fully precipitated the dispersion, obtaining a yellow powder exhibiting a strong green emission when excited with ultraviolet (UV) of 367 nm wavelength (inset of Figure 1b; Figure S1, Supporting Information). This is in contrast to common bulk-like perovskite crystals, which typically only show weak emission.[25] We then employed high angle annular dark field scanning transmission electron microscopy (HAADF-STEM) and were able to image particles several hundreds of nanometers in size (Figure 1b), thus explaining the observed precipitation. However, under closer inspection it turned out that these were not single large crystals, but were actually comprised of smaller cubic NCs roughly 10 nm in size (Figure 1c,d; Figure S2, Supporting Information). This could be seen more clearly in bright field transmission electron microscopy (BF-TEM) and HAADF-STEM images acquired, also reveals a typical spacing range of 0.75–1.5 nm between the NCs (Figure 1d; Figure S2, Supporting Information). A fast Fourier transformation (FFT) of the image clearly represents the cubic close packing of the crystalline nanocubes in these large crystal superlattices (Figure 1d). The polyhedral nature of these 200–400 nm large SCs could be observed nicely in scanning electron microscopy images (SEM), although care had to be given to prevent the structures from degrading under the electron beam (Figure S3, Supporting Information).[25,47] In addition, X-ray diffraction of the individual $CsPbBr_3$ NCs and of the SCs revealed similar diffraction patterns, which can be assigned to either cubic or orthorhombic crystal structures (Figure S4, Supporting Information). The clearer peaks from the SCs are likely due to the larger concentration of material in the measured powders.

In addition to 3D SCs, we also observed some self-assembled monolayers of $CsPbBr_3$ nanocubes in the STEM images (Figure S2, Supporting Information). These monolayers likely form spontaneously during the drying process from individual NCs present in the concentrated colloidal dispersion. In fact this process has been widely enforced to obtain large-area 2D and 3D self-assemblies of metal and semiconductor NCs on solid surfaces. By contrast, the spontaneous self-assembly of NCs into well-defined SCs in colloidal dispersions has only been rarely observed.[48,49] The self-assembly process of the SCs in the dispersions is likely governed by the van der Waals attraction between the hydrophobic ligands and the perovskite NC cores under high colloidal concentration. Such spontaneous self-assembly processes have been previously observed in the formation of free-standing SCs of polyhedral gold NCs.[49]

In order to elucidate the formation process of the perovskite SCs out of the precursor powders, we monitored the PL spectra of the reaction product during the synthesis (**Figure 2**a). Images of the vials illuminated with white light can be found in Figure S1 of the Supporting Information. For the first 5 min, there is only little if any PL observable. At 5 min we observe a broad PL signal, with distinct shoulders at 499 and 526 nm. While the latter peak corresponds to the PL emission of bulk $CsPbBr_3$, the former peak likely stems from smaller NCs exhibiting quantum-confinement. As the reaction progresses, the shoulder decreases in intensity and redshifts up to 512 nm, becoming nearly indistinguishable at 30 min. This value corresponds to that seen previously for weakly confined $CsPbBr_3$ NCs.[1,24,50] The main peak gradually redshifts to 535 nm during the course of the synthesis. This was quite surprising as the reported PL maxima for $CsPbBr_3$ NCs exhibit a maximum wavelength of 520 nm, even for non-quantum confined NCs (sizes > 10 nm).[14,24] It instead resembles that of bulk macrocrystals of $CsPbBr_3$[38] and thin films.[51]

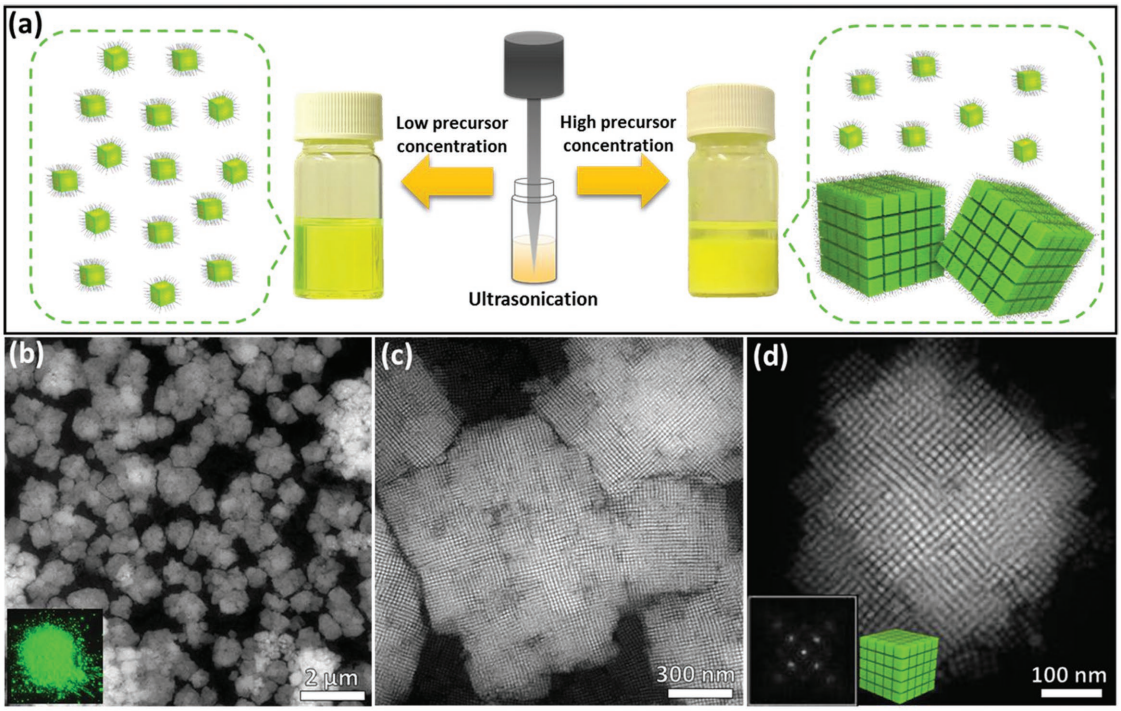

Figure 1. a) Schematic illustration of the synthesis of $CsPbBr_3$ perovskite NCs by single-step tip sonication of precursor salts in octadecene in the presence of oleic acid and oleylamine and images of the respective dispersions under ambient light. The reaction yields well-dispersed individual NCs at low precursor concentration (left side), while it results in the formation of self-assembled SCs for high precursor concentrations (right side). b,c) HAADF-STEM images of the colloidal SCs with different magnifications. (Inset of b: photograph of SC powder under UV light illumination.) d) Magnified HAADF-STEM image of a single $CsPbB_3$ perovskite SC (inset: selected area FFT pattern of the SC).

To understand the origin of these spectra, we acquired BF-TEM images on material extracted from the synthesis at specific times during the synthesis (Figure 2b–d). After 5 min many individual NCs can be seen along with some smaller clusters with largest contrast, indicating the formation of small SCs. As the synthesis progresses, the single NCs vanish, being replaced by larger and larger SCs, with an increasing contrast consistent with their increasing lateral sizes. Thus the redshift of the PL spectra is concomitant with the increase in the SC size. Interestingly, upon dilution of these SC dispersions, the PL position blueshifts again, nearly to the position of the NCs formed under lower concentrations (Figure S5a, Supporting Information). TEM imaging confirms that the dilution leads to split up of the SCs, resulting in predominantly separated NCs with a few small NC aggregates dispersed in between (Figure S5c,d, Supporting Information). The difference in emission wavelength can be seen even more clearly in PL spectra acquired from dense films fabricated from the NCs and SCs (Figure 2e). The PL is redshifted by 21 to 535 nm for the SC film, with a small shoulder remaining at 516, and likely stemming from single NCs present in the SC dispersion. Since the NCs basically remain separated instead of fusing together, the observed shift must stem from an electronic coupling between the individual NCs. Possibilities for such coupling have been studied in literature previously, although often on SCs of epitaxially grown quantum dots.[36,37,52] In a similar way as the atoms interact in an atomic solid, the electronic wavefunctions of the individual semiconductor NCs can interact strongly in a perovskite SC, provided a small enough spacing, which in turn can lead to the formation of minibands in both valence and conduction bands, as illustrated in Figure 2f.[36] Such miniband formation in SCs leads to a lowering of the lowest-energy optical transition, which is seen in the redshift of the PL as compared with individual NCs.[39] Studies on 2D perovskites show that miniband formation should be observable at separation distances comparable to those obtained for the supercrystals.[53] Previous studies have shown that the redshift in the PL emission of perovskites can also be caused by reabsorption.[54] However, reabsorption only affects the PL and not the absorption (or PLE), as initially emitted photons are reabsorbed with subsequently emitted photons being redshifted to the originally emitted ones. This leads to a narrowing of the PL signal with a reduction on the short wavelength side and a concomitant increase on the long wavelength side. In our case, we observe a strong redshift of the PLE onset from the NCs to the SCs accompanied by a similar redshift of the PL signal (see Figure S6, Supporting Information). As the width of the PL peaks are nearly identical, we can rule out reabsorption as a major effect in our system. In addition, the results show that the redshift in the PL peak position is quite significant at the initial stages of the SC growth. As the number of NCs in the SCs increases, the redshift only increases slightly (Figure 2a). This is due to the fact that electronic coupling is significant only among nearest neighbors.

In addition, it is worth mentioning that it was easy to prepare films of SCs compared to the films made of uncoupled

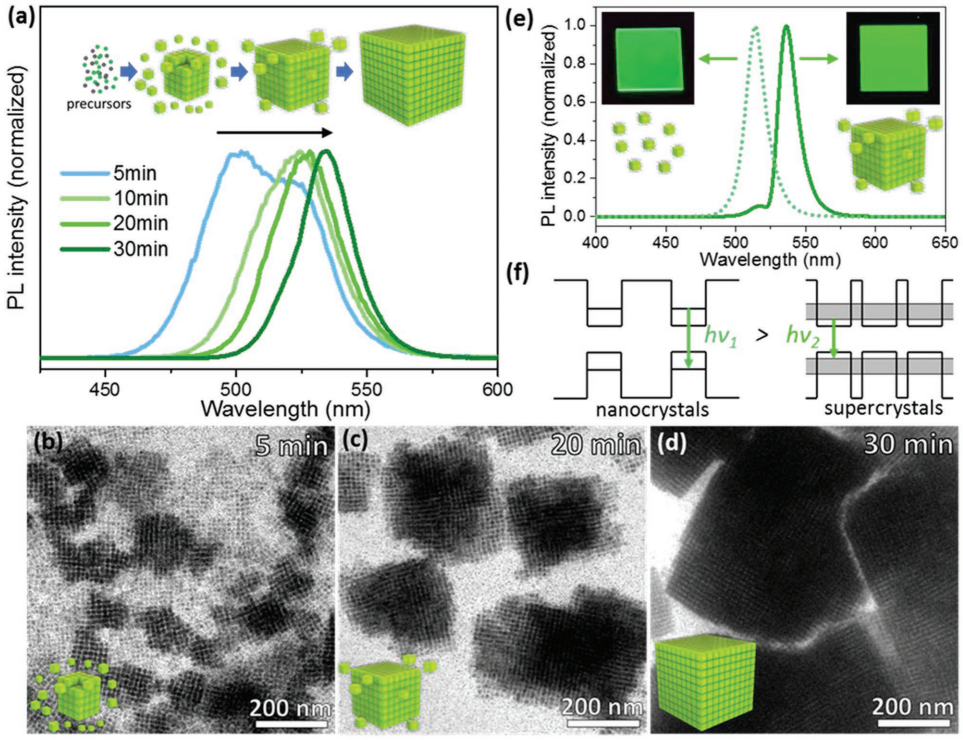

Figure 2. a) PL spectra of the $CsPbBr_3$ perovskite colloidal dispersion obtained at different reaction times during the transformation of precursor powders into SCs by ultrasonication. Inset: Schematic illustration of the gradual transformation of precursor powders into 3D SCs of $CsPbBr_3$ nanocubes. b–d) BF-TEM images of the crystals present after 5, 20, and 30 min of synthesis time. e) PL spectra of perovskite films of individual NCs (left side) and SCs (right side). Insets are photos of the films under UV-light illumination. f) Energy diagram of the corresponding situations. While the NCs remain electronically isolated (left side), the individual NCs inside the SCs couple together leading to miniband formation and a redshift of the emission wavelength.

NCs, because of the high concentration of colloids in SC dispersion. Another reason for this is that the purification of SCs by centrifugation is a lot easier due to their heavy mass, whereas it is difficult to separate the excess ligands from the well-dispersed NCs. The SCs can be prepared in high concentration colloidal dispersion for its use in the fabrication of dense films by spin-coating. The PL emission wavelength of the films made of SCs greatly depends on the concentration of the colloidal solution used for their fabrication (Figure S7, Supporting Information). If the solutions are diluted before spin-coating, the SCs disassemble, resulting in a blueshift of the PL emission peak. More importantly, despite the SCs being highly purified, with nearly no residual ligand remaining in the dispersions, the films made of SCs are highly emissive with a PLQY of 45%, even slightly surpassing that of the NC films, which exhibited a PLQY of ≈40%. The quantum yield in the films is lower than in the dispersions. This is likely due to partial ligand desorption, which occurs during the rigorous purification which is necessary to obtain high quality films. Apparently, the self-assembly of NCs into SCs is not detrimental on the PLQY. This is extremely interesting, as both the films comprising larger NCs (≈100 nm) and bulk thin films exhibited extremely low PLQYs of 0.5% and <0.1%, respectively (Figure S8, Supporting Information). Thus, the redshifted emission typical of bulk-sized $CsPbBr_3$ perovskite structures can be merged together with the superior PLQY of weakly confined NCs in the SCs. These superior properties of SCs make them unique for light emitting applications, as compared with bulk films.

The commonly used method of halide ion exchange to shift the optical bandgap and PL emission of perovskite NCs is easily applicable to the SCs (**Figure 3**a; Figure S9, Supporting Information).[22,23] Similarly to the bromide case, strongly luminescing powders can be obtained with a clear color difference depending on halide content. The ion exchange process turned out to be significantly slower than for the individual NC dispersion, likely due to the halide ions having to permeate the dense SCs in order to replace the original halide ions for all NCs. Importantly, the halide ion exchange reaction basically preserves the SC morphology as confirmed by TEM characterization (Figure S10, Supporting Information) despite a partial disassembly of the SCs upon dilution in the solutions required for ion exchange. As shown in Figure 3b,c, the absorption onset and PL emission peaks of films fabricated out of the $CsPbX_3$ SCs gradually blueshift with increasing chloride amount and redshift as the iodide content increases. The PL spectra of all perovskite SC films (solid lines) show the same redshift in comparison to the individual NC solutions (dashed lines), so that they likely all exhibit electronic coupling. The SC films containing Br and I ions exhibit relatively high PLQYs around 45%, whereas the Cl-containing samples exhibit low

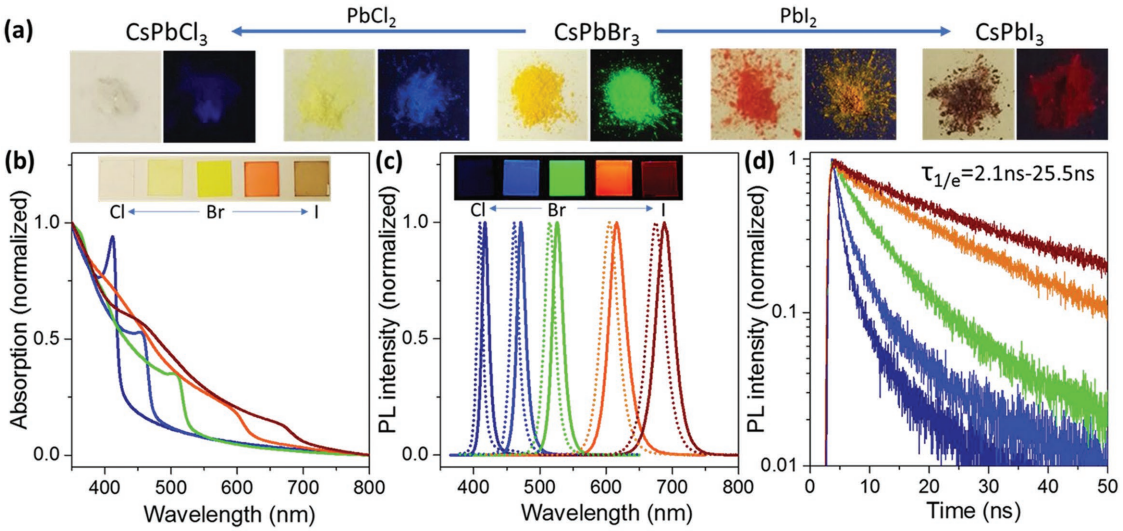

Figure 3. a) Photographs of the powders of $CsPbX_3$ perovskite SCs with different halide compositions under room light (left side) and UV light illumination (right side). b) UV-vis absorption spectra of perovskite films made by spin-coating concentrated colloidal dispersion diluted colloidal SC dispersions. c) The corresponding PL spectra (solid line) in comparison with those of films of isolated NCs. (Insets of (b) and (c): photographs of the perovskite SC films under room light and UV illumination, respectively.) d) PL decay dynamics of the SC films shown in (c). The PL lifetime increases with increasing emission wavelength from 2.1 to 25.5 ns.

PLQYs of around 10%. Time-resolved PL measurements revealed that going from iodide to chloride via bromide the decay becomes faster. This halide composition-dependent PL decay trend for SCs is similar to that of individual NCs, as observed by us and others.[1,24] Recent studies have shown that a large part of this is due to a difference in nonadiabatic charge-phonon coupling.[55] Due to the higher mass in iodides and the resulting slower movement, this coupling is reduced, leading to a nonradiative decay rate which increases from iodides to bromides to chlorides as is observed in this study. A concomitant increase of the radiative decay rate from iodide to bromide to chloride leads to a further quickening of the PL decay.[55] These results suggest that the SCs can be employed for integration into optoelectronic devices due to their excellent optical properties, high yield, and stability.

One problem in thin film LEDs is currently the lack of a true green emitter with high quantum yield. This dearth has been dubbed the "green gap."[34] $CsPbBr_3$ NCs have proven to be promising materials for light emitting application owing to their facile synthesis with high PLQY. The number of research articles is increasing, which focused on the fabrication and optimization of perovskite LEDs based either on $CsPbBr_3$ thin films or NCs.[7,8,56] While the thin films show a color spectrum close to the desired Rec2020 standard, they exhibit low PLQYs (Figure S9, Supporting Information). The bromide-based NCs on the other hand have quite high efficiencies, however, due to a weak quantum confinement, their emission color is shifted further away from the desired region.[10,24,57] As shown in this work, the $CsPbBr_3$ perovskite SCs exhibit an emission wavelength further shifted toward the recommended green (Rec2020) color. Hence, we now explore the fabrication of pure green LEDs on both rigid as well as on flexible substrates using the SCs as the emitting layer. One of the advantages of using perovskites in LEDs is the ability to use solution process. This means that the active layers can be deposited via spin-coating the corresponding solution, providing a simple and cost-effective approach for fabricating LEDs. In most previous studies on perovskite NC-based LEDs, the carrier transport layers on top of perovskite nanocrystal films were deposited via thermal evaporation, because the NCs are easily washed away by organic solvents if they are not properly cross-linked.[58] Here, we have successfully employed a solution-processed electron transport layer poly(ethyleneimine) (PEI)/ZnO on top of the perovskite film without affecting the perovskite SCs film using ZnO dispersed in ethyl acetate instead of toluene. The schematic illustration of the fabricated LED device architecture and the SEM image of the corresponding device cross-section are presented in **Figure 4**a (see Figure S11 of the Supporting Information for top-view images of the individual layers). An extremely thin PEI layer was introduced by spin-coating for stabilizing the perovskite layer as well as modifying the work function of ZnO.[59] The fabricated LED displays bright PL at 527 nm and a strong bright green electroluminescence (EL) at 3 V, slightly redshifted to 529 nm (a photo in the inset of Figure 4b). These peaks are only slightly blueshifted from the SC film emission position of 536 nm due to the partial disassembly of SCs in the diluted solution used for spin-coating (Figure S7, Supporting Information). A corresponding version of this LED, but using isolated $CsPbBr_3$ NCs was fabricated and showed the expected blueshifted EL emission (Figure S12, Supporting Information). The SC based EL device shows stable EL, with a gradual increase in intensity with increasing driving voltage up to 7 V, while nearly retaining the peak position (Figure S13, Supporting Information). As can be seen in Figure 4c, which is based on the CIE (International Commission on Illumination) 1931 color coordinator, the SC-based LED exhibits a color closer to the recommended pure green

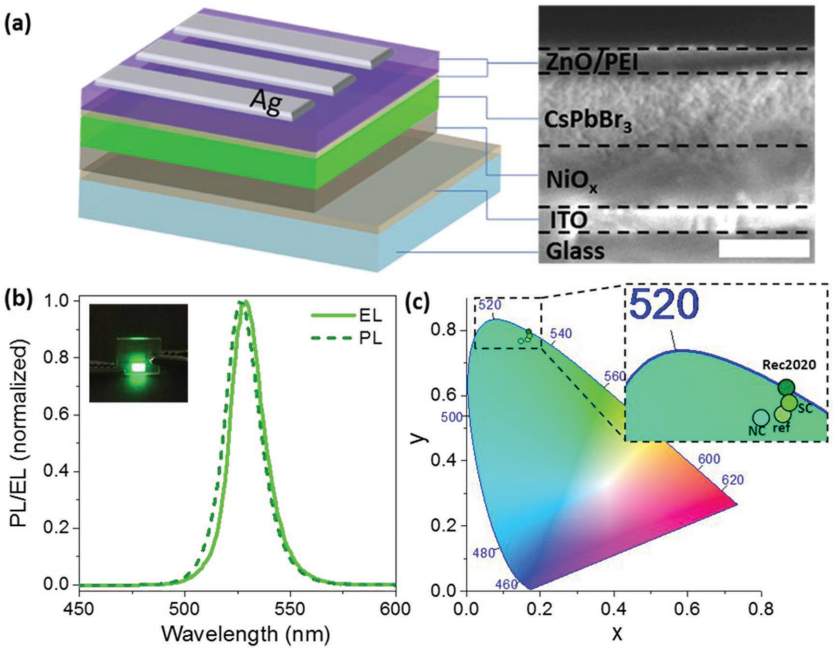

Figure 4. a) Device architecture and cross-sectional SEM image of the $CsPbBr_3$ perovskite LED device. The scale bar corresponds to 500 nm. b) The EL and PL spectra of the $CsPbBr_3$ perovskite SC (insets: photograph of the corresponding LED device showing EL). c) CIE coordinates of the SC LED device (inset: magnified view of the color coordinates of $CsPbBr_3$ SCs (SC), isolated NCs of $CsPbBr_3$ (NC), and $FAPbBr_3$ (ref) in comparison with the recommended pure green (Rec2020) color).

(Rec2020), in comparison to the $CsPbBr_3$ NC LED and also to that of a device based on formamidinium lead bromide ($FAPbBr_3$) NCs.[60] These results clearly indicate that the charges can tunnel through the ligand barrier of coupled NCs and recombine radiatively to emit green light. We also fabricated flexible LEDs on PET film instead of glass substrate using both NCs and SCs (Figure S14, Supporting Information). This worked for both the NCs and SCs and the devices showed similar characteristics to those employing the rigid substrates. Together, these results highlight the promise of using perovskite SCs for display applications.

In summary, we have presented the spontaneous self-assembly of perovskite NCs into highly emissive SCs from precursor powders in a highly concentrated solution. Both steps, NC synthesis and self-assembly take place simultaneously in one pot. We have found that the perovskites SCs exhibit a redshifted PL emission due to electronic coupling of the wavefunctions in neighboring NCs and the resulting formation of minibands. The redshift in the PL of $CsPbBr_3$ SCs makes them pure green emitters, which is demonstrated by the fabrication of pure green EL-LED devices on rigid and even flexible substrates. Importantly, despite the more bulk-like emission wavelength, the SCs retain the high PLQY of the NCs. The optical properties of the perovskite SCs are tunable across the visible spectrum by applying the common halide ion exchange reaction on the $CsPbBr_3$ SC-templates. The results presented in this work show the promise of the colloidal solution of SCs for solution-processed light emitting applications.

Supporting Information

Supporting Information is available from the Wiley Online Library or from the author.

Acknowledgements

This research work was supported by the Bavarian State Ministry of Science, Research, and Arts through the grant "Solar Technologies go Hybrid (SolTech)," by the China Scholarship Council (Y.T. and K.W.), by the European Union's Horizon 2020 research and innovation program under the Marie Skłodowska-Curie Grant Agreement COMPASS No. 691185 and by LMU Munich's Institutional Strategy LMUexcellent within the framework of the German Excellence Initiative (L.P., J.F. and A.S.U.). E.B. and S.B. acknowledge financial support from the European Research Council (ERC Starting Grant #335078-COLOURATOMS). The authors would like to thank Alexander Richter for helpful discussions.

Conflict of Interest

The authors declare no conflict of interest.

Keywords

$CsPbX_3$ perovskite, electronic coupling, green LEDs., supercrystals, superlattices

Received: February 16, 2018
Revised: April 14, 2018
Published online: June 5, 2018

[1] L. Protesescu, S. Yakunin, M. I. Bodnarchuk, F. Krieg, R. Caputo, C. H. Hendon, R. X. Yang, A. Walsh, M. V. Kovalenko, *Nano Lett.* **2015**, *15*, 3692.
[2] M. V. Kovalenko, L. Protesescu, M. I. Bodnarchuk, *Science* **2017**, *358*, 745.
[3] L. Dou, A. B. Wong, Y. Yu, M. Lai, N. Kornienko, S. W. Eaton, A. Fu, C. G. Bischak, J. Ma, T. Ding, N. S. Ginsberg, L.-W. Wang, A. P. Alivisatos, P. Yang, *Science* **2015**, *349*, 1518.
[4] S. D. Stranks, G. E. Eperon, G. Grancini, C. Menelaou, M. J. P. Alcocer, T. Leijtens, L. M. Herz, A. Petrozza, H. J. Snaith, *Science* **2013**, *342*, 341.
[5] G. Xing, N. Mathews, S. Sun, S. S. Lim, Y. M. Lam, M. Grätzel, S. Mhaisalkar, T. C. Sum, *Science* **2013**, *342*, 344.
[6] Q. A. Akkerman, M. Gandini, F. Di Stasio, P. Rastogi, F. Palazon, G. Bertoni, J. M. Ball, M. Prato, A. Petrozza, L. Manna, *Nat. Energy* **2016**, *2*, 16194.
[7] Y. Zhang, J. Liu, Z. Wang, Y. Xue, Q. Ou, L. Polavarapu, J. Zheng, X. Qi, Q. Bao, *Chem. Commun.* **2016**, *52*, 13637.
[8] H. Huang, L. Polavarapu, J. A. Sichert, A. S. Susha, A. S. Urban, A. L. Rogach, *NPG Asia Mater.* **2016**, *8*, e328.
[9] Y. Wang, X. Li, J. Song, L. Xiao, H. Zeng, H. Sun, *Adv. Mater.* **2015**, *27*, 7101.
[10] L. Polavarapu, B. Nickel, J. Feldmann, A. S. Urban, *Adv. Energy Mater.* **2017**, *7*, 1700267.

[11] X. Li, Y. Wang, H. Sun, H. Zeng, *Adv. Mater.* **2017**, *29*, 1701185.
[12] L. C. Schmidt, A. Pertegas, S. Gonzalez-Carrero, O. Malinkiewicz, S. Agouram, G. M. Espallargas, H. J. Bolink, R. E. Galian, J. Perez-Prieto, *J. Am. Chem. Soc.* **2014**, *136*, 850.
[13] A. Swarnkar, V. K. Ravi, A. Nag, *ACS Energy Lett.* **2017**, *2*, 1089.
[14] A. Swarnkar, R. Chulliyil, V. K. Ravi, M. Irfanullah, A. Chowdhury, A. Nag, *Angew. Chem., Int. Ed.* **2015**, *54*, 15424.
[15] J. Liu, Y. Xue, Z. Wang, Z.-Q. Xu, C. Zheng, B. Weber, J. Song, Y. Wang, Y. Lu, Y. Zhang, Q. Bao, *ACS Nano* **2016**, *10*, 3536.
[16] F. Zhang, H. Zhong, C. Chen, X.-g. Wu, X. Hu, H. Huang, J. Han, B. Zou, Y. Dong, *ACS Nano* **2015**, *9*, 4533.
[17] H. Huang, F. Zhao, L. Liu, F. Zhang, X.-g. Wu, L. Shi, B. Zou, Q. Pei, H. Zhong, *ACS Appl. Mater. Interfaces* **2015**, *7*, 28128.
[18] M. C. Weidman, M. Seitz, S. D. Stranks, W. A. Tisdale, *ACS Nano* **2016**, *10*, 7830.
[19] X. Zhang, H. Lin, H. Huang, C. Reckmeier, Y. Zhang, W. C. H. Choy, A. L. Rogach, *Nano Lett.* **2016**, *16*, 1415.
[20] M. Chen, Y. T. Zou, L. Z. Wu, Q. Pan, D. Yang, H. C. Hu, Y. S. Tan, Q. X. Zhong, Y. Xu, H. Y. Liu, B. Q. Sun, Q. Zhang, *Adv. Funct. Mater.* **2017**, *27*, 1701121.
[21] Y. Bekenstein, B. A. Koscher, S. W. Eaton, P. D. Yang, A. P. Alivisatos, *J. Am. Chem. Soc.* **2015**, *137*, 16008.
[22] G. Nedelcu, L. Protesescu, S. Yakunin, M. I. Bodnarchuk, M. J. Grotevent, M. V. Kovalenko, *Nano Lett.* **2015**, *15*, 5635.
[23] Q. A. Akkerman, V. D'Innocenzo, S. Accornero, A. Scarpellini, A. Petrozza, M. Prato, L. Manna, *J. Am. Chem. Soc.* **2015**, *137*, 10276.
[24] Y. Tong, E. Bladt, M. F. Aygüler, A. Manzi, K. Z. Milowska, V. A. Hintermayr, P. Docampo, S. Bals, A. S. Urban, L. Polavarapu, J. Feldmann, *Angew. Chem., Int. Ed.* **2016**, *55*, 13887.
[25] J. A. Sichert, Y. Tong, N. Mutz, M. Vollmer, S. Fischer, K. Z. Milowska, R. García Cortadella, B. Nickel, C. Cardenas-Daw, J. K. Stolarczyk, A. S. Urban, J. Feldmann, *Nano Lett.* **2015**, *15*, 6521.
[26] V. A. Hintermayr, A. F. Richter, F. Ehrat, M. Döblinger, W. Vanderlinden, J. A. Sichert, Y. Tong, L. Polavarapu, J. Feldmann, A. S. Urban, *Adv. Mater.* **2016**, *28*, 9478.
[27] Y. Tong, F. Ehrat, W. Vanderlinden, C. Cardenas-Daw, J. K. Stolarczyk, L. Polavarapu, A. S. Urban, *ACS Nano* **2016**, *10*, 10936.
[28] Q. A. Akkerman, S. G. Motti, A. R. Srimath Kandada, E. Mosconi, V. D'Innocenzo, G. Bertoni, S. Marras, B. A. Kamino, L. Miranda, F. De Angelis, A. Petrozza, M. Prato, L. Manna, *J. Am. Chem. Soc.* **2016**, *138*, 1010.
[29] Y. Bekenstein, B. A. Koscher, S. W. Eaton, P. Yang, A. P. Alivisatos, *J. Am. Chem. Soc.* **2015**, *137*, 16008.
[30] D. Zhang, S. W. Eaton, Y. Yu, L. Dou, P. Yang, *J. Am. Chem. Soc.* **2015**, *137*, 9230.
[31] Y. Tong, B. J. Bohn, E. Bladt, K. Wang, P. Müller-Buschbaum, S. Bals, A. S. Urban, L. Polavarapu, J. Feldmann, *Angew. Chem., Int. Ed.* **2017**, *56*, 13887.
[32] H. Huang, B. Chen, Z. Wang, T. F. Hung, A. S. Susha, H. Zhong, A. L. Rogach, *Chem. Sci.* **2016**, *7*, 5699.
[33] S. Pathak, N. Sakai, F. Wisnivesky Rocca Rivarola, S. D. Stranks, J. Liu, G. E. Eperon, C. Ducati, K. Wojciechowski, J. T. Griffiths, A. A. Haghighirad, A. Pellaroque, R. H. Friend, H. J. Snaith, *Chem. Mater.* **2015**, *27*, 8066.
[34] F. Nippert, S. Y. Karpov, G. Callsen, B. Galler, T. Kure, C. Nenstiel, M. R. Wagner, M. Straßburg, H.-J. Lugauer, A. Hoffmann, *Appl. Phys. Lett.* **2016**, *109*, 161103
[35] I. Lignos, L. Protesescu, D. B. Emiroglu, R. Maceiczyk, S. Schneider, M. V. Kovalenko, A. J. deMello, *Nano Lett.* **2018**, *18*, 1246.
[36] T. Sugaya, T. Amano, M. Mori, S. Niki, *Appl. Phys. Lett.* **2010**, *97*, 043112.
[37] M. Scheibner, T. Schmidt, L. Worschech, A. Forchel, G. Bacher, T. Passow, D. Hommel, *Nat. Phys.* **2007**, *3*, 106.
[38] Y. Rakita, N. Kedem, S. Gupta, A. Sadhanala, V. Kalchenko, M. L. Böhm, M. Kulbak, R. H. Friend, D. Cahen, G. Hodes, *Cryst. Growth Des.* **2016**, *16*, 5717.
[39] J. Zhang, A. A. Lutich, A. S. Susha, M. Döblinger, C. Mauser, A. O. Govorov, A. L. Rogach, F. Jäckel, J. Feldmann, *J. Appl. Phys.* **2010**, *107*, 123516.
[40] Z. Nie, A. Petukhova, E. Kumacheva, *Nat. Nanotechnol.* **2009**, *5*, 15.
[41] C. R. Kagan, C. B. Murray, *Nat. Nanotechnol.* **2015**, *10*, 1013.
[42] M. P. Pileni, *J. Phys. Chem. B* **2001**, *105*, 3358.
[43] Y. Min, M. Akbulut, K. Kristiansen, Y. Golan, J. Israelachvili, *Nat. Mater.* **2008**, *7*, 527.
[44] L. Motte, F. Billoudet, E. Lacaze, M.-P. Pileni, *Adv. Mater.* **1996**, *8*, 1018.
[45] M. Grzelczak, J. Vermant, E. M. Furst, L. M. Liz-Marzán, *ACS Nano* **2010**, *4*, 3591.
[46] N. Soetan, W. R. Erwin, A. M. Tonigan, D. G. Walker, R. Bardhan, *J. Phys. Chem. C* **2017**, *121*, 18186.
[47] Z. Dang, J. Shamsi, F. Palazon, M. Imran, Q. A. Akkerman, S. Park, G. Bertoni, M. Prato, R. Brescia, L. Manna, *ACS Nano* **2017**, *11*, 2124.
[48] L.-X. Dai, X.-Y. Wang, X.-Y. Zheng, Y.-W. Zhang, *Chem. Commun.* **2016**, *52*, 5023.
[49] C.-W. Yang, C.-Y. Chiu, M. H. Huang, *Chem. Mater.* **2014**, *26*, 4882.
[50] D. N. Dirin, I. Cherniukh, S. Yakunin, Y. Shynkarenko, M. V. Kovalenko, *Chem. Mater.* **2016**, *28*, 8470.
[51] Y. Li, Z.-F. Shi, S. Li, L.-Z. Lei, H.-F. Ji, D. Wu, T.-T. Xu, Y.-T. Tian, X.-J. Li, *J. Mater. Chem. C* **2017**, *5*, 8355.
[52] D. V. Talapin, J.-S. Lee, M. V. Kovalenko, E. V. Shevchenko, *Chem. Rev.* **2010**, *110*, 389.
[53] J. Even, L. Pedesseau, C. Katan, *ChemPhysChem* **2014**, *15*, 3733.
[54] L. M. Pazos-Outón, M. Szumilo, R. Lamboll, J. M. Richter, M. Crespo-Quesada, M. Abdi-Jalebi, H. J. Beeson, M. Vrućinić, M. Alsari, H. J. Snaith, B. Ehrler, R. H. Friend, F. Deschler, *Science* **2016**, *351*, 1430.
[55] J. He, A. S. Vasenko, R. Long, O. V. Prezhdo, *J. Phys. Chem. Lett.* **2018**, *9*, 1872.
[56] J. Song, J. Li, X. Li, L. Xu, Y. Dong, H. Zeng, *Adv. Mater.* **2015**, *27*, 7162.
[57] L. Protesescu, S. Yakunin, M. I. Bodnarchuk, F. Bertolotti, N. Masciocchi, A. Guagliardi, M. V. Kovalenko, *J. Am. Chem. Soc.* **2016**, *138*, 14202.
[58] G. Li, F. W. R. Rivarola, N. J. L. K. Davis, S. Bai, T. C. Jellicoe, F. de la Peña, S. Hou, C. Ducati, F. Gao, R. H. Friend, N. C. Greenham, Z.-K. Tan, *Adv. Mater.* **2016**, *28*, 3528.
[59] S. Woo, W. Hyun Kim, H. Kim, Y. Yi, H.-K. Lyu, Y. Kim, *Adv. Energy Mater.* **2014**, *4*, 1301692.
[60] S. Kumar, J. Jagielski, N. Kallikounis, Y.-H. Kim, C. Wolf, F. Jenny, T. Tian, C. J. Hofer, Y.-C. Chiu, W. J. Stark, T.-W. Lee, C.-J. Shih, *Nano Lett.* **2017**, *17*, 5277.